Article

Cell Stem Cell

TPO-Induced Metabolic Reprogramming Drives Liver Metastasis of Colorectal Cancer CD110+ Tumor-Initiating Cells

Graphical Abstract

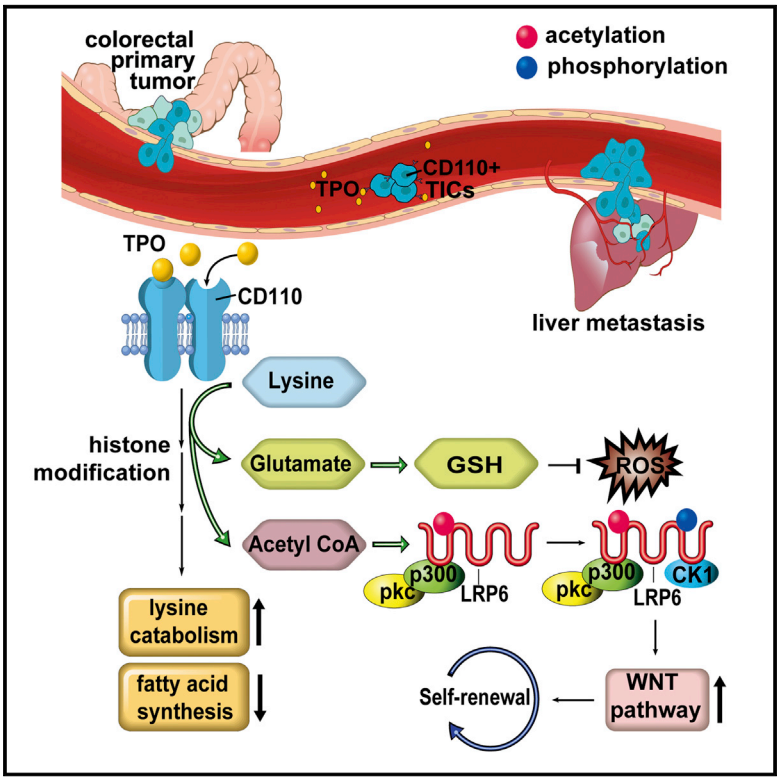

Authors

ZhengMing Wu, Dong Wei, WenChao Gao, ..., ChunFang Gao, XiaoYan Zhu, QingQuan Li

Correspondence

061101040@fudan.edu.cn

In Brief

Liver metastasis is a leading cause of death for colorectal cancer patients. In this study, Wu et al. show that metabolic reprogramming in colorectal cancer tumor-initiating cells to enhance lysine metabolism is a key step in this process and is mediated by the soluble environmental factor thrombopoietin.

Highlights

- Colorectal CD110+ cancer cells in liver metastases show enhanced lysine degradation
- TPO-mediated activation of lysine degradation is required for liver metastasis
- Lysine catabolism leads to activated Wnt signaling and a shift in redox status
- TPO-induced c-*myc* recruits chromatin modifiers to regulate gene expression

Accession Numbers

GSE64595

Wu et al., 2015, Cell Stem Cell *17*, 47–59
July 2, 2015
http://dx.doi.org/10.1016/j.stem.2015.05.016

CellPress

Cell Stem Cell
Article

TPO-Induced Metabolic Reprogramming Drives Liver Metastasis of Colorectal Cancer CD110+ Tumor-Initiating Cells

ZhengMing Wu,[1,6] Dong Wei,[2,6] WenChao Gao,[3,6] YuTing Xu,[1] ZhiQian Hu,[3] ZhenYu Ma,[4] ChunFang Gao,[2] XiaoYan Zhu,[5] and QingQuan Li[1,*]
[1]Department of Pathology, Shanghai Medical College, Fudan University, Shanghai 200032, China
[2]Department of Anus and Intestine Surgery, PLA Central Hospital 150, Luoyang, Henan 471031, China
[3]Department of General Surgery, Changzheng Hospital, Second Military Medical University, Shanghai 200003, China
[4]Department of General Surgery, Huashan Hospital, Fudan University, Shanghai 200040, China
[5]Department of Traditional Chinese Medicine, Shanghai Cancer Hospital, Fudan University, Shanghai 200032, China
[6]Co-first author
*Correspondence: 061101040@fudan.edu.cn
http://dx.doi.org/10.1016/j.stem.2015.05.016

SUMMARY

Liver metastasis is a leading cause of death in patients with colorectal cancer. We previously found that colorectal cancer tumor-initiating cells (TICs) expressing CD110, the thrombopoietin (TPO)-binding receptor, mediate liver metastasis. Here, we show that TPO promotes metastasis of CD110+ TICs to the liver by activating lysine degradation. Lysine catabolism generates acetyl-CoA, which is used in p300-dependent LRP6 acetylation. This triggers tyrosine phosphorylation of LRP6, ultimately activating Wnt signaling to promote self-renewal of CD110+ TICs. Lysine catabolism also generates glutamate, which modulates the redox status of CD110+ TICs to promote liver colonization and drug resistance. Mechanistically, TPO-mediated induction of c-*myc* orchestrates recruitment of chromatin modifiers to regulate metabolic gene expression. Our findings, therefore, establish TPO as a component of the physiological environment critical for metastasis of colorectal cancer to the liver.

INTRODUCTION

Liver metastasis is the leading cause of death in patients with colorectal cancer (CRC). The seeding and the outgrowth of distant metastasis of cancer are dependent on tumor-initiating cells (TICs) (Visvader and Lindeman, 2008; Pang et al., 2010)—particularly, migrating TICs, a subset of TICs with a mesenchymal phenotype (Tang, 2012). A specialized microenvironment, referred to as a metastatic niche, is critical for allowing the outgrowth of metastatic nodules from migrating TICs (Oskarsson et al., 2014), but the niche components supporting liver metastasis are mostly unknown.

In a previous study, we showed that migrating TICs that drive liver metastasis of CRC express CD110, a thrombopoietin (TPO)-responsive homodimeric receptor (Gao et al., 2013). The self-renewal of hematopoietic stem cells requires a balance between positive and negative signals downstream of the TPO/CD110 axis (Fox et al., 2002). Considering that TICs and stem cells share many common features and that liver is the major organ producing TPO (Vigon et al., 1992), we speculated that TPO is a niche component critical for liver metastasis of CRC. TPO recruits CD110+TICs to the liver and promotes their self-renewal in a paracrine manner (Gao et al., 2013). Such a finding is consistent with the fact that CRC rarely metastasizes to the liver in patients with chronic hepatitis and, therefore, low TPO levels (Martin et al., 1997; Wang et al., 2012). Further support for the pro-metastatic role of TPO comes from studies suggesting that interleukin-6 (IL-6) produced in advanced stages of CRC (Knüpfer and Preiss, 2010) could increase hepatic TPO production and cause thrombocytosis (Kaser et al., 2001), which, in turn, is an independent risk factor for CRC metastasis (Voutsadakis, 2014). In the current study, we examined the molecular mechanism(s) by which hepatic TPO promotes liver colonization of CD110+TICs.

RESULTS

Lysine Catabolism Is Increased in CD110+TICs in Liver Metastatic Lesions

In a previous study using an in vivo model of organ-specific metastasis of CRC, we showed that CD110+TICs are responsible for liver metastasis (Gao et al., 2013). In the current study, we compared a transcription profile of CD110+ tumor cells derived from the primary xenograft of two CRC liver metastasis cell lines (CRC102-LM and CRC108-LM) with those from liver metastasis, using global transcriptome analysis (Figure 1A). The highest ranking genes were validated by qPCR (Figure S1A). In the KEGG (Kyoto Encyclopedia of Genes and Genomes) analysis, the top enriched pathways included the p53 signaling pathway, Wnt signaling pathway, and saccharopine pathway (lysine degradation) (Figure 1B). A pilot experiment that inhibited each of the three pathways showed the most robust reduction in liver colonization by CD110+TICs upon inhibition of lysine catabolism (Figure S1B). Transcripts for most enzymes in lysine catabolism (AASS, AASDH, AADAT, BCKDH, ECHS1, and HMGCL) and for lysine transporters (CAT1 and CAT2B) were increased

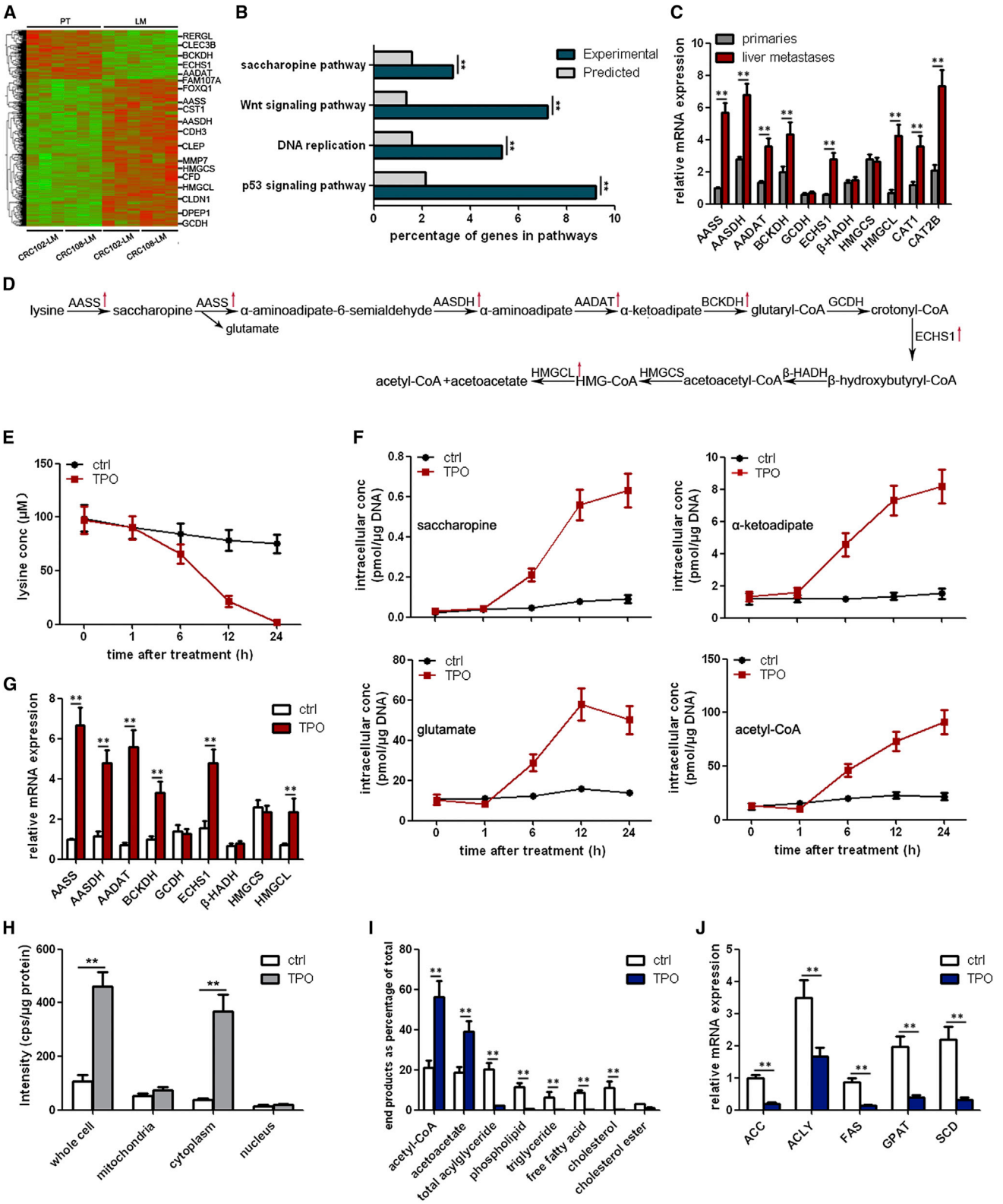

Figure 1. TPO Initiates Lysine Catabolism in Colorectal CD110+TICs

(A) Comparison of gene expression profiles between CD110+TICs from primary tumors (PT) and from liver metastases (LM).

(B) KEGG pathway analysis showing differential gene expression between CD110+TICs from liver metastases and from primary tumors. L, liver parenchyma; M, metastatic lesion.

(legend continued on next page)

(Figures 1C and 1D). Consistent with the transcriptome results, lysine degradation was also elevated in CD110+ cells from peripheral blood of mice with CRC102-LM and CRC108-LM tumors (Figure S2A).

Next, we tested whether the TPO-CD110 axis initiates the metabolic reprogramming in CD110+TICs. In comparison with differentiated tumor cells, TICs are more dependent on glycolysis (Mao et al., 2013). In our experiments, both CD133+CD110+ and CD133+CD110− subpopulations from primary CRC102 tumors had a higher glycolytic rate than the corresponding CD133− cells. TPO treatment of CD110+ cells decreased lysine concentration in culture medium via increased cellular uptake (Figure 1E), without impairing glycolysis (Figure S2B). A significant increase in the intracellular level of metabolic intermediates in lysine metabolism (e.g., saccharopine, α-ketoadipate, glutamate, and acetyl-coenzyme A [acetyl-CoA]) was observed as early as 6 hr after TPO treatment (Figure 1F). The expression of most enzymes involved in lysine catabolism showed a concurrent increase (Figures 1G and S2C). Differentiating CD110+TICs with serum significantly reduced the amount of lysine consumption following TPO exposure (Figure S2D). This metabolic reprogramming could be reversed by TPO withdrawal (Figure S2E). Similar results were obtained with primary CRC105 tumor (data not shown).

Lysine degradation generates acetyl-CoA, which, in turn, serves as a precursor in the citric acid cycle in mitochondria as well as participates in fatty acid synthesis in cytoplasm and histone acetylation in cell nucleus. Upon incubation of CD110+ cells with ^{13}C-Lys and TPO, we observed an increase in cytoplasmic acetyl-CoA (Figure 1H). Unexpectedly, only <5% of lysine was converted to fatty acid (Figure 1I). Expression of fatty acid synthesis enzymes (ACC, ACLY, FAS, GPAT, and SCD) was suppressed (Figures 1J and S2C). ^{13}C-Lys metabolism provided 58.3% of the acetyl-CoA for the TPO-treated CD110+ cells, in contrast to 21.6% prior to TPO treatment (Figure 1I). Therefore, acetyl-CoA was the main end product of lysine metabolism.

Lysine Catabolism Is Indispensable for Liver Colonization by CD110+TICs

Next, we examined the expression of AASS, the rate-limiting enzyme in the lysine catabolism, in human samples of primary CRC and metastatic nodules. AASS was positive in 82.3% of liver metastatic nodules, 8.2% of primary tumors, and only 2.3% of lung metastatic lesions. No AASS expression was detected in metastatic samples from lymph nodes and peritoneum (Figure 2A). In liver metastatic nodules, AASS staining was more evident at the invasive edge (Figure 2B). Higher AASS expression in liver nodules was associated with shorter time to liver relapse after resection (Figures 2C and S3) and poorer overall survival (Figure 2C). The classic saccharopine pathway predominates in the liver (Papes et al., 1999). Although AASS staining was strongly positive in healthy liver parenchyma, its expression was significantly lower in tumor-adjacent liver tissues (Figure 2D). AASS expression was significantly higher in CD110+ metastatic samples than in CD110− metastases (Figure 2E). Immunofluorescence staining suggested colocalization of AASS with CD110 in liver metastases but not in primary lesions (Figure 2F). These results implied that lysine catabolism is essential for liver colonization by CD110+TICs.

In NOG (NOD/Shi-scid/IL-2Rgnull) mice orthotopically implanted with CD110+ cells overexpressing GFP, dietary lysine deprivation inhibited 90% of liver metastasis (Figure 2G) but failed to affect tumor growth (Figure S4A), primary tumor entry into circulation (Figure S4B, upper panel), or tumor cell extravasation from blood vessels (Figure S4B, lower panel). In a previous study (Gao et al., 2013), we showed that CDCP1+ cells drive CRC metastasis to the lungs. In the current study, we transduced parental CRC102 cells with retroviral vectors expressing a short hairpin RNA (shRNA) targeting AASS under the control of a promoter element responsive to either CD110 (cis-CD110-HSV1-tk/shAASS) or CDCP1 (cis-CDCP1-HSV1-tk/shAASS) and implanted transduced cells orthotopically into NOG mice on a normal diet. AASS knockdown decreased liver metastasis (Figure S4D, upper panel) without affecting primary tumor formation (Figure S4C, upper panel), intravasation (Figure S4C, lower panel), or lung metastasis (Figure S4D, lower panel). To examine the role of lysine metabolism during different phases of liver metastasis, we generated CD110+ cells expressing AASS shRNA under the control of a doxycycline (Dox)-dependent promoter (Figure S5A) and injected these cells via tail vein into mice on a normal diet. Observation of liver colonization for various periods of time prior to Dox administration revealed increased liver metastatic burden (Figures 2H and 2I). CD110+AASS+ cells were uniformly distributed throughout micrometastases soon after liver colonization. As the colonies grew, these cells progressively segregated to the invasive front (Figure 2I). Dox administration starting at 2 days or 7 days after inoculation inhibited micrometastasis outgrowth and increased CD110+ cell apoptosis. In stark contrast, Dox administration starting at 28 days after inoculation, when metastatic nodules were large, did not affect metastatic burden or survival of CD110+ cells (Figures 2H, S5B, and S5C). Therefore, lysine catabolism plays an important role in the formation of micrometastases but not late metastatic foci.

Acetyl-CoA Derived from Lysine Catabolism Transfers the Acetyl Group to LRP6 in a p300-Dependent Manner

TPO promotes CD110+TICs to self-renew, an essential capacity for early metastasis (Gao et al., 2013). In the current study, we found increased self-renewal of CD110+TICs in lysine-containing,

(C) Validation of upregulated lysine catabolism genes in CD110+TICs from liver metastases.
(D) Schematic diagram of genes encoding enzymes involved in lysine degradation that are significantly upregulated in CD110+TICs from liver metastases.
(E) Effects of TPO (0.1 ng/ml) on lysine consumption by CD110+ cells.
(F) Effects of TPO (0.1 ng/ml) on intracellular levels of saccharopine, α-ketoadipate, glutamate, and acetyl-CoA in CD110+ cells. conc, concentration.
(G) CD110+ cells from CRC102 were treated with 0.1 ng/ml TPO for 6 hr, and expression of lysine catabolism genes was measured using qPCR. CD110+ cells from CRC105 were incubated with 0.1 ng/ml TPO and ^{13}C-Lys for 6 hr.
(H) The amount and distribution of ^{13}C-acetyl-CoA were measured by mass spectrometry and normalized to protein concentration. cps, counts per second.
(I) End products, quantified as a percentage of total radioactive end products, were measured by mass spectrometry.
(J) CD110+ cells from CRC105 were treated with 0.1 ng/ml TPO for 6 hr. Expression of fatty acid synthesis genes was measured using qPCR.
Values are mean ± SD. **$p < 0.05$. See also Figures S1 and S2.

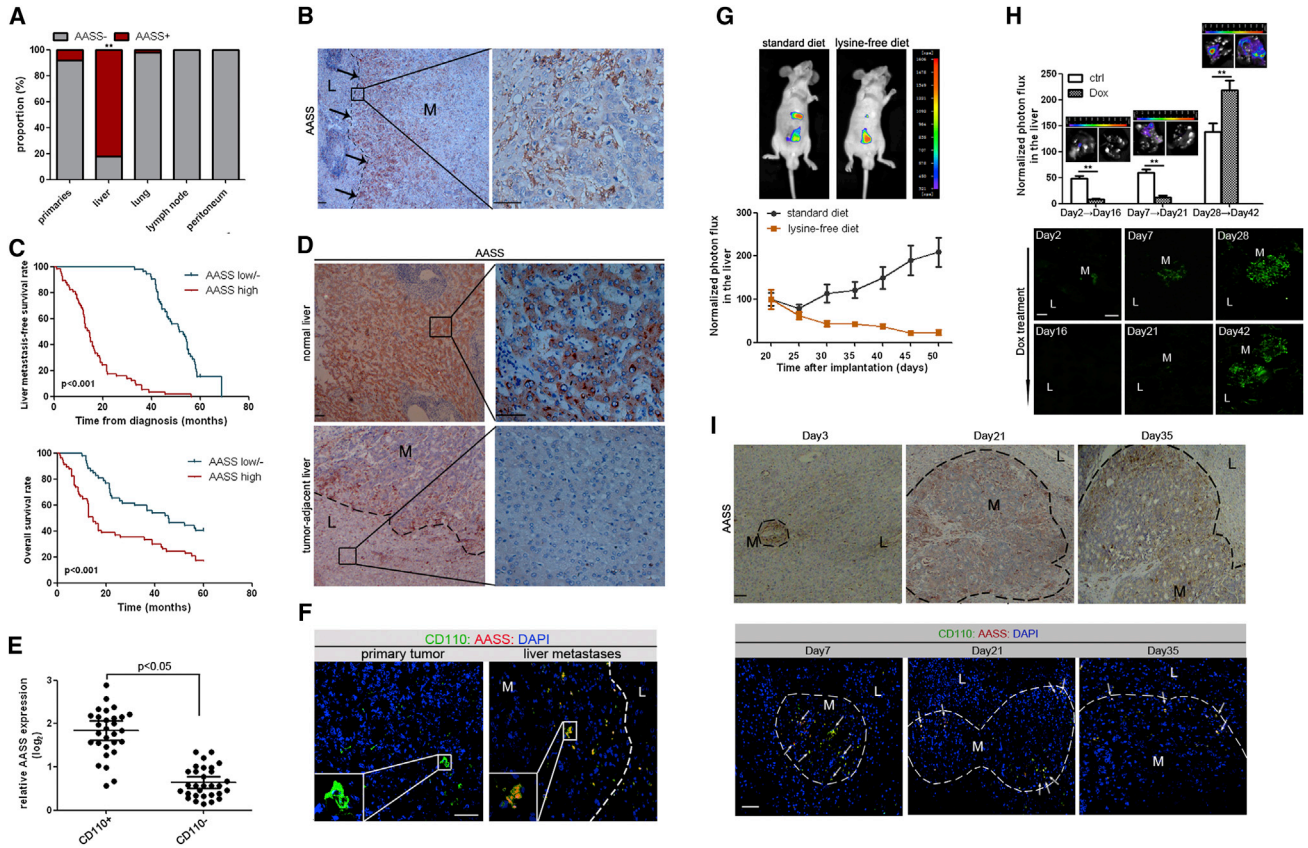

Figure 2. Lysine Degradation Is Involved in Early Liver Colonization by CD110+TICs

(A) Proportion of AASS-positive cases in clinical samples from primary colorectal tumors (n = 64), liver metastases (n = 52), lung metastases (n = 23), lymph node metastases (n = 25), and peritoneum metastases (n = 9).

(B) AASS immunostaining (arrows) in liver metastases from a patient with colorectal cancer.

(C) Kaplan-Meier analysis of liver metastasis-free survival (upper panel) and overall survival (lower panel) of patients with colorectal cancer on the basis of AASS expression in liver metastases.

(D) Immunohistochemical analysis of AASS expression in normal liver and tumor-adjacent liver tissues.

(E) Relative levels of AASS expression in CD110− versus CD110+ liver metastasis samples.

(F) Co-immunofluorescent (co-IF) staining of AASS and CD110 in primary tumors and liver metastases.

(G) Mice were implanted orthotopically with CD110+ cells from CRC102-LM and then were randomized into groups receiving a standard or lysine-free diet (n = 5 per group). Representative bioluminescence images (upper panel) and bioluminescence quantification of liver sections (lower panel) are shown at different time points. CD110+TICs expressing GFP were allowed to colonize the liver for different lengths of time before Dox (40 mg/kg) was administered to knock down AASS.

(H) Bioluminescence analysis (upper panel) and GFP imaging (lower panel) of liver colonization at the indicated time points.

(I) Immunostaining of AASS (upper panel) and co-IF analysis of AASS and CD110 expression (lower panel) in liver metastases at different time points.

Values are mean ± SD. **p < 0.05. Scale bars, 50 μm. See also Figures S3–S5.

but not in lysine-free, medium upon TPO treatment. Such effect of lysine deprivation was rescued by adding either lysine or its metabolic intermediates (α-aminoadipate or α-ketoadipate) but not by adding acetoacetate (Figure 3A). The rescuing action of self-renewal by α-aminoadipate or α-ketoadipate was attenuated by knocking down HMGCL (Figure 3B), an enzyme that catalyzes the cleavage of HMG-CoA to acetoacetate and acetyl-CoA (Figure 1D).

Acetyl-CoA is a major acetyl donor in the acetylation of histones and non-histone proteins (Kaochar and Tu, 2012). Considering acetyl-CoA accumulation in cytoplasm (Figure 1H), we spiked the TPO-treated CD110+ cells with ^{13}C-lysine and immunoprecipitated acetylated peptides from cytoplasmic extracts to identify candidates containing ^{13}C-acetyllysine. One of the proteins identified was LRP6, a co-receptor of Wnt signaling crucial for self-renewal of colon TICs (Vermeulen et al., 2010). In our experiments, the temporal profile of LRP6 acetylation synchronized with cytoplasmic acetyl-CoA increase (Figure 3C). LRP6 was no longer acetylated in an AASS or HMGCL mutant (Figure 3D). In CRC xenografts derived from CRC102-LM or CRC105-LM cell lines, LRP6 acetylation was detectable in CD110+TICs from liver metastases but not from primary lesions (Figure S6A). Mass spectrometry of co-immunoprecipitated samples revealed an interaction of LRP6 with p300, a histone acetyltransferase (Ogryzko et al., 1996). The association between p300 and LRP6 was prominent upon TPO exposure but lost in the absence of TPO (Figure 3E). Transduction of CD110+TICs with either shRNA targeting p300 or a

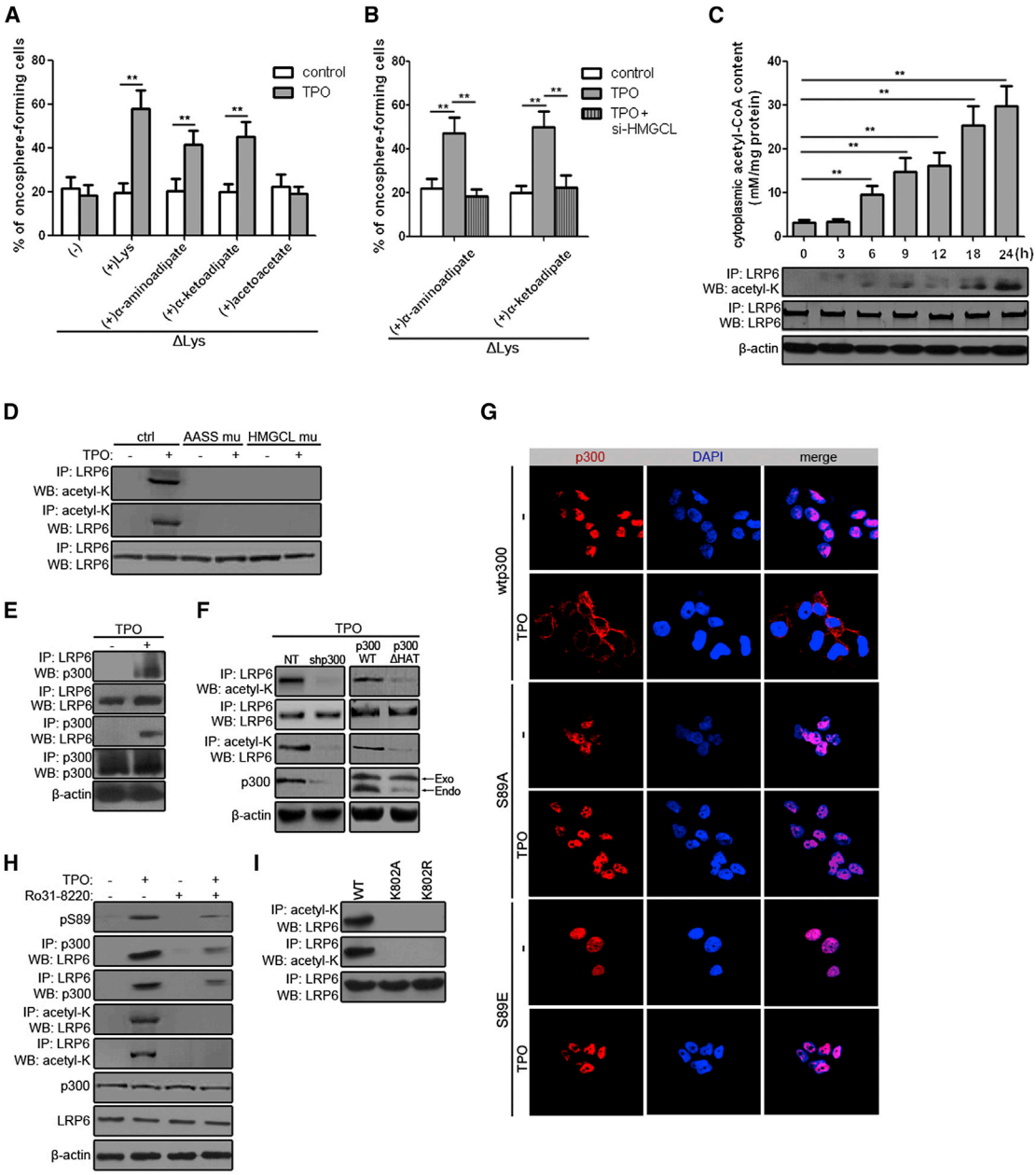

Figure 3. Lysine Degradation Provides Acetyl-CoA to Acetylate LRP6 in a p300-Dependent Manner

(A) CD110+ cells from CRC108 were cultured in lysine-deprived medium (ΔLys) and treated with 0.1 ng/ml TPO for 7 days. Cells were supplemented with 100 μM lysine, α-aminoadipate, α-ketoadipate, or acetoacetate; and the percentage of oncosphere-forming cells was determined.

(B) CD110+ cells from CRC108 cultured in lysine-deprived medium (ΔLys) were treated for 7 days with 0.1 ng/ml TPO and/or a siRNA against HMGCL. Cells were supplemented with 100 μM α-aminoadipate or α-ketoadipate, and the percentage of oncosphere-forming cells was determined.

(C) Time course of cytoplasmic acetyl-CoA content (upper panel) and LRP6 acetylation (lower panel) in TPO-treated CD110+ cells. LRP6 acetylation was measured by western blotting (WB) of the immunoprecipitated proteins as indicated. IP, immunoprecipitation.

(D) LRP6 acetylation in response to TPO (0.1 ng/ml) in CD110+ cells expressing AASS or HMGCL mutant (mu).

(E) Co-immunoprecipitation (Co-IP) of LRP6 and p300 in CD110+ cells treated with or without 0.1 ng/ml TPO for 48 hr.

(F) LRP6 acetylation in CD110+ cells treated with 0.1 ng/ml TPO and/or a shRNA against p300 or ΔHAT for 48 hr. WT, wild-type.

(G) IF staining of p300 in CD110+ cells expressing wild-type p300 or S89 mutants, following TPO treatment (0.1 ng/ml).

(H) Co-IP analysis of acetylated LRP6 and the p300-LRP6 complex in CD110+ cells treated for 48 hr with 0.1 ng/ml TPO and/or 5 μM Ro-31-8220.

(I) LRP6 acetylation in CD110+ cells expressing wild-type LRP6 or K802 mutants, following TPO treatment (0.1 ng/ml).

Values are mean ± SD. **p < 0.05. See also Figure S6.

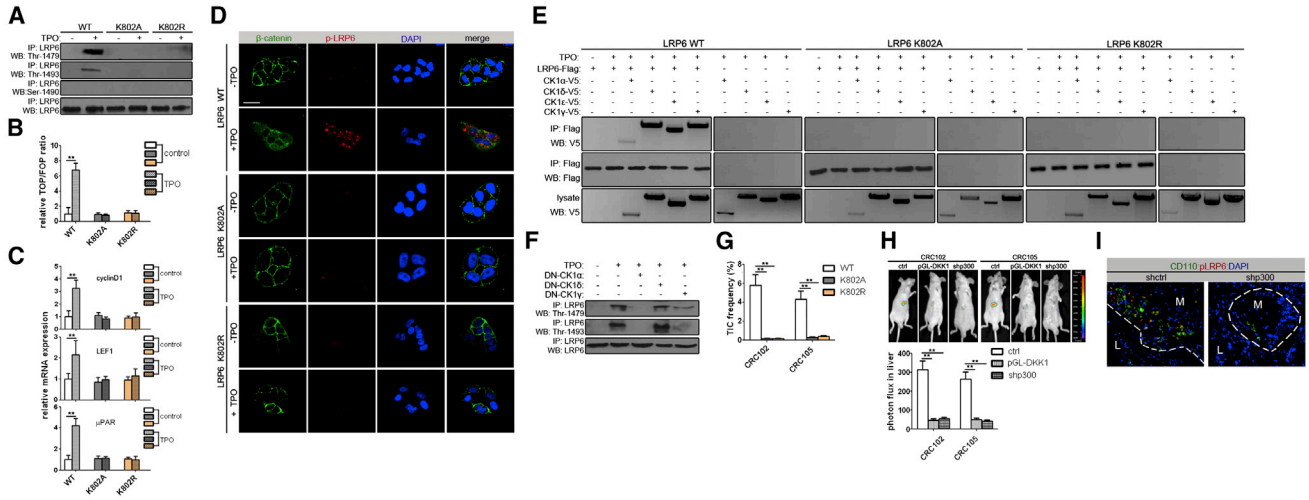

Figure 4. Effects of LRP6 Acetylation on LRP6 Activity and Self-Renewal of CD110+TICs

CD110+ cells expressing wild-type LRP6 or K802 mutants were cultured for 48 hr in the presence or absence of 0.1 ng/ml TPO.

(A) Phosphorylation of T1479, T1493, and S1490 was analyzed by western blotting (WB) of co-IP as indicated. WT, wild-type; IP, immunoprecipitation.

(B) Transcriptional activity of the TOP/FOP reporter plasmid was analyzed by luciferase reporter assays.

(C) Representative confocal images of β-catenin (green) and phosphorylated LRP6 (red).

(D) Expression of mRNA encoding Wnt target genes (*cyclinD1*, *LEF1*, and *μPAR*) was measured using qPCR.

(E) Co-IP analysis of the LRP6-CK1 complex in CD110+ cells expressing LRP6-flag (200 ng), K802A-flag (200 ng), K802R-flag (200 ng), and/or V5-CK1 (200 ng), following treatment with TPO (0.1 ng/ml).

(F) Phosphorylation of T1479 and T1493 in CD110+ cells expressing DN-CK1 (200 ng) following treatment with TPO (0.1 ng/ml).

(G) TIC frequency of CD110+TICs co-expressing pcDNA3.0-TPO and wild-type LRP6 or K802 mutants was measured by limiting dilution assays in vivo.

(H and I) Liver colonization (H) and LRP6 phosphorylation in liver metastases (I) were determined by bioluminescence and IF in mice injected intravenously with control (ctrl) CD110+ cells from CRC102 and CRC105 or cells transduced with pGL-DKK1 or shRNA against p300.L, liver parenchyma; M, metastatic lesion.

Values are mean ± SD. $^{**}p < 0.05$. Scale bar, 10 μm. See also Figure S6.

catalytically inactive p300 mutant (ΔHAT) decreased TPO-induced LRP6 acetylation (Figure 3F).

P300 has been reported to localize exclusively in the nucleus (Ogryzko et al., 1996). Surprisingly, p300 moved from the nucleus into the cytoplasm when CD110+ cells were treated with TPO in our experiments (Figure 3G). Protein kinase C (PKC) represses transcriptional activity by phosphorylating p300 on S89 (Yuan and Gambee, 2000). The TPO/CD110 axis regulates PKC signaling (Hong et al., 1998). Therefore, we generated p300 mutants in which S89 was replaced with A or Q and expressed them in CD110+ cells. In the presence of TPO, both S89 mutants showed abundant nuclear localization but no detectable cytoplasmic staining (Figure 3G). The PKC inhibitor Ro31-8220 blocked TPO-induced S89 phosphorylation, reduced the amount of p300 that co-immunoprecipitated with LRP6, and inhibited LRP6 acetylation (Figure 3H), suggesting that PKC signaling is required for TPO-induced p300-LRP6 interaction and LRP6 acetylation.

To identify the specific site(s) of TPO-induced acetylation on LRP6, we overexpressed flag-tagged LRP6 in CD110+ cells. Tandem mass spectrometry analysis identified an acetylation site at K802 upon TPO treatment (Figure S6B). To confirm this result, we generated LRP6 mutants in which K802 was replaced with A or R and expressed these mutants in CD110+ cells. Upon TPO treatment, acetylation was evident in wild-type LRP6 but not either K802 mutants (Figure 3I). Next, we transfected wild-type LRP6 or K802 mutants into CD110+ cells and orthotopically implanted these cells into NOG mice. K802 mutation markedly decreased liver colonization (Figure S6D, right panel) but did not affect primary tumor formation (Figure S6C) or intravasation by CD110+TICs (Figure S6D, left panel).

LRP6 Acetylation Stimulates LRP6 Activity and Self-Renewal of CD110+TICs

Activation of LRP6 in canonical Wnt signaling requires phosphorylation (Bilic et al., 2007). In our experiments with CD110+TICs, TPO led to LRP6 phosphorylation at two key residues (Thr1479 and 1493), whereas no phosphorylation of K802 mutants was detectable (Figure 4A). Consistent with the functional importance of LRP6 phosphorylation, TPO treatment of K802 mutant-expressing cells failed to activate TOP-FLASH reporter expression (Figure 4B) and, therefore, did not affect β-catenin accumulation in the cytosol (Figure 4D) and transcription of Wnt target genes (Figure 4C). Both LRP6 phosphorylation (Figure S6E, left panel) and Wnt signaling activity (Figure S6E, right panel) were higher in CD110+TICs from liver metastases than from primary lesions. Next, we focused on casein kinase (CK), which typically recognizes putative phosphorylation sites of LRP6 (Davidson et al., 2005). TPO induced all four CK1s (CK1α/ε/δ/γ) to co-immunoprecipitate with wild-type but not the K802 LRP6 mutants (Figure 4E). Dominant-negative (DN)-CK1α and DN-CK1γ, but not DN-CK1δ, blocked TPO-induced LRP6 phosphorylation (Figure 4F).

To determine the role of acetylated LRP6 on self-renewal of CD110+TICs, we gave mice limiting doses of CD110+ cells that co-express exogenous TPO with wild-type LRP6 or K802

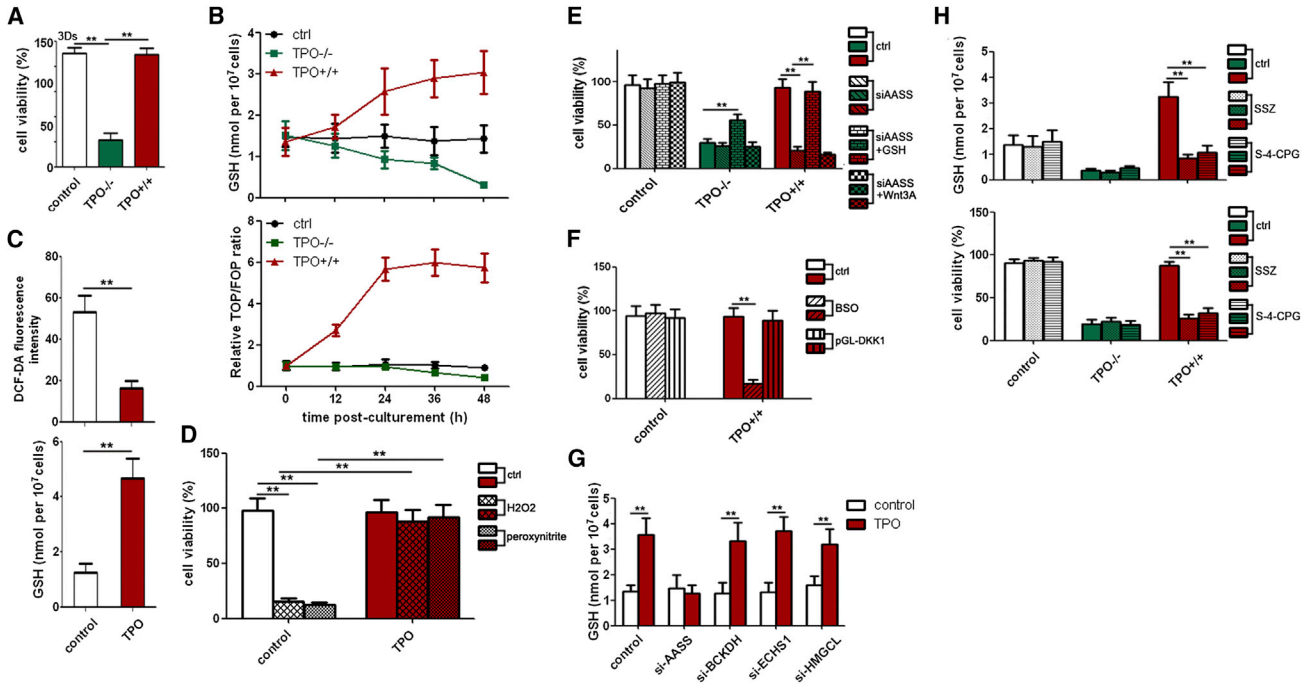

Figure 5. Lys → Glu Metabolism Promotes Survival of CD110+TICs during Liver Colonization

(A) CD110+ cells from CRC105 were co-cultured with ischemic $TPO^{+/+}$ or $TPO^{-/-}$ livers for 3 days, and then cell viability was measured by flow cytometry. 3Ds, 3 days.

(B) GSH content (upper panel) and activity of TOP/FOP reporter plasmid (lower panel) in CD110+ cells co-cultured with ischemic $TPO^{+/+}$ versus $TPO^{-/-}$ livers.

(C) Effects of TPO (0.1 ng/ml; 72 hr) on intracellular ROS (upper panel) and GSH (lower panel) in CD110+ cells. DCF-DA, 2′,7′-dichlorofluoresein diacetate.

(D) CD110+ cells were cultured for 72 hr with 0.1 ng/ml TPO and/or H_2O_2 (100 μM) or peroxynitrite (200 μM), and then cell viability was measured by flow cytometry.

(E) CD110+ cells from the experiment in Figure 5A were treated with siRNA against AASS, AASS siRNA together with GSH (2 mM), or AASS siRNA together with Wnt3A conditional medium. The cell viability was assessed by flow cytometry. ctrl, control.

(F) After treatment with BSO (10 nM) or pGL-DKK1, CD110+ cells were co-cultured with ischemic $TPO^{+/+}$ livers for 3 days, and cell viability was measured by flow cytometry.

(G) Comparison of GSH level in CD110+ cells treated for 72 hr with 0.1 ng/ml TPO and/or siRNA against AASS, BCKDH, ECHS1, or HMGCL.

(H) CD110+ cells from the experiment in Figure 5A were also treated for 3 days with SSZ (50 μM) or S-4-CPG (25 μM), after which GSH content (upper panel) and cell viability (lower panel) were determined.

Values are mean ± SD. **$p < 0.05$.

mutants. Tumors generated from a single CD110+ cell (with limiting dilution) were transplanted into secondary recipients (Figure S6F). When compared to the wild-type group, there was a >10-fold decrease in the frequency of self-renewing cells in the K802 mutant groups (Figure 4G). Suppression of LRP6 activity, either by overexpressing Dickkopf-1 (Dkk1) (Niehrs, 2006) or by knocking down p300 expression (Figure S6G), decreased liver metastatic efficiency (Figure 4H). Immunohistochemistry on liver metastases showed a decreased number of CD110+pLRP6+ cells in mice treated with shp300 (Figure 4I). These results suggest that p300-mediated acetylation is indispensable for LRP6 activation to support metastatic colonization by CD110+TICs.

TPO Reduces Oxidative Stress in CD110+TICs via the Lys-Glu Pathway

Oxidative stress caused by tumor arrest in hepatic sinusoids and reperfusion limits cancer metastasis (Jessup et al., 1999). In this study, we induced hepatic ischemia in $TPO^{+/+}$ or $TPO^{-/-}$ mice by clamping the hepatic artery and portal vein for 3 min. Glutathione (GSH) is one of the most important antioxidant defenses against oxidative stress in cancer cells. Within 3 days, primary CD110+ cultures with $TPO^{-/-}$ ischemic livers showed substantial cell death, with a time-dependent decrease in GSH. Co-culturing these cells with $TPO^{+/+}$ ischemic livers significantly enhanced cell viability and increased GSH (Figure 5A; Figure 5B, upper panel). Adding TPO to cultured CD110+ cells decreased intracellular reactive oxygen species (ROS) (Figure 5C, upper panel), increased GSH (Figure 5C, lower panel), and decreased their sensitivity to exogenous ROS (H_2O_2) or peroxynitrite (Figure 5D). Wnt/β-catenin signaling protects cells against oxidative stress (Tao et al., 2013). Wnt signaling activity in CD110+ cells was higher upon co-incubation with $TPO^{+/+}$ than with $TPO^{-/-}$ ischemic liver (Figure 5B, lower panel). The loss of CD110+ cell viability upon AASS knockdown was rescued by the supplement of glutathione but not Wnt3A (Figure 5E). Consistently, the protective effect of TPO was diminished by GSH depletion and not affected by Wnt pathway inhibition (Figure 5F). Glutamate is a by-product of lysine degradation and upregulates GSH synthesis (Richman and Meister, 1975). In CD110+ cells treated with

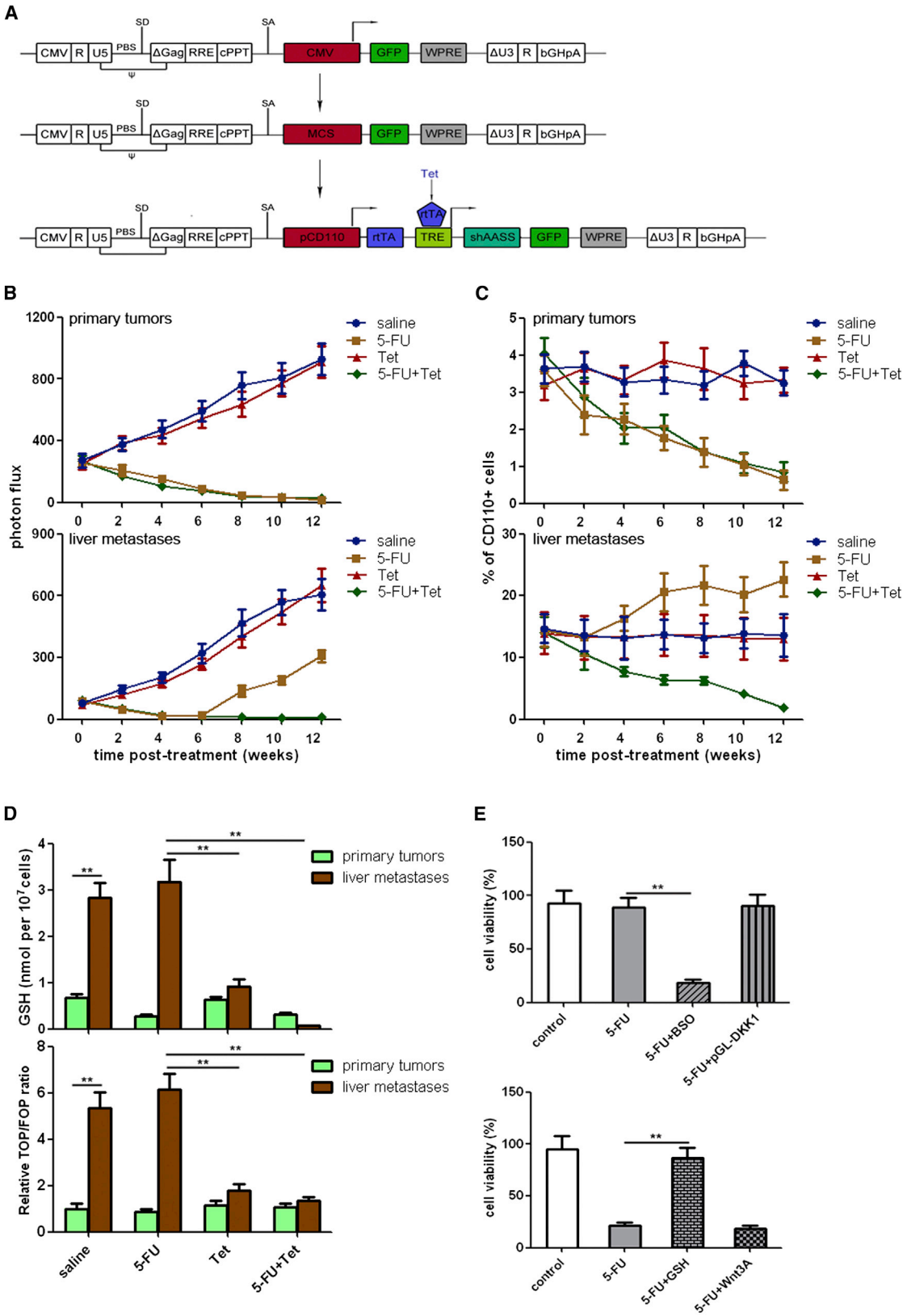

(legend on next page)

TPO, intracellular GSH was reduced by knockdown of AASS but not BCKDH, ECHS1, or HMGCL (Figure 5G). System x_c^- imports cystine into cells in exchange for glutamate to provide cysteine, the rate-limiting substrate in GSH synthesis (Lewerenz et al., 2013). Adding the structurally unrelated system x_c^- inhibitor sulfasalazine or S-4-carboxyphenylglycine abolished TPO-induced GSH production (Figure 5H, upper panel) and sensitized CD110+ cells to $TPO^{+/+}$ ischemic livers (Figure 5H, lower panel).

Many chemotherapeutic agents, including fluorouracil (5-FU), produce antitumor activity by promoting ROS-dependent apoptosis (Sangeetha et al., 1990). In this experiment, CRC102-LM cells were transfected with a lentiviral vector in which the shRNA targeting AASS is under the dual control of the CD110-responsive promoter and the Tet-inducible activator rtTA (referred to as pCRTA; Figure 6A) and were orthotopically transplanted into NOG mice. Upon establishment of liver metastases 4 weeks later, mice were treated with 5-FU alone, Tet alone, or 5-FU plus Tet. Treatment with 5-FU alone produced >82% tumor regression at week 6 (Figure 6B) but significantly increased the percentage of CD110+ cells in liver metastases (Figure 6C, lower panel). Recurrence (n = 7 for liver and n = 1 for peritoneum) was noted in 8 out of 10 such mice. In these cases, both GSH level and Wnt activity were higher in CD110+ cells in liver metastases than those in primary lesions (Figure 6D). Next, we examined the relative contribution of GSH versus Wnt signaling. The sensitivity of cultured CD110+ cells to 5-FU was greatly enhanced by GSH depletion with buthionine sulfoximine (BSO) but not Wnt inhibition with DKK1 overexpression (Figure 6E, upper panel). Tet treatment alone did not affect the development of tumor burden (Figure 6B), but it decreased GSH level, as well as Wnt activity, in CD110+ cells from liver metastases (Figure 6D). In stark contrast, treatment with 5-FU plus Tet decreased the size of liver metastases (Figure 6B, lower panel) as well as the percentage of CD110+ cells in liver metastatic lesions (Figure 6C, lower panel). In vivo, Tet treatment enhanced the sensitivity of isolated CD110+ cells to 5-FU exposure in a manner dependent on GSH and not Wnt (Figure 6E, lower panel). Therefore, recurrence was not noted in any subject.

TPO-Induced c-*myc* Recruits HBO1 to Mediate Acetylation of H3K14 in Genes Encoding Enzymes Involved in Lysine Catabolism and Fatty Acid Synthesis

c-myc is essential in the TPO-CD110 axis in stem cells (Chanprasert et al., 2006). In our experiments, c-*myc* expression was significantly upregulated by TPO, before lysine degradation became detectable (1 hr versus 6 hr) (Figure 7A). Chromatin immunoprecipitation-qPCR (ChIP-qPCR) (Figure S7A, upper panel) and qRT-PCR analyses (Figure S7A, lower panel) revealed TPO-induced binding of endogenous c-*myc* to promoters of most, if not all, genes encoding enzymes involved in lysine degradation and fatty acid synthesis. We examined the effects of TPO treatment on the changes of histone markers. TPO increased H3K14 acetylation in CD110+ cells in a c-*myc*-dependent manner, without affecting other histone markers (Figure 7B). H3K14 acetylation is a hallmark of active transcription (Koch et al., 2007). ChIP-qPCR analysis of c-*myc* binding sites in two genes involved in lysine metabolism (AASS and BCKDH) and two genes encoding enzymes involved in fatty acid synthesis (ACC and FAS) showed that c-*myc* increased acetylation of H3K14 on these promoters (Figure 7C). This increase was observed regardless of whether the genes were activated or repressed. Confocal imaging showed nearly complete overlap between c-*myc* and acetylated H3K14 in the nuclei of TPO-treated CD110+ cells (Figure 7D).

HBO1 is required for most H3K14 acetylation events in mammals (Kueh et al., 2011). As anticipated, we found binding of HBO1 and c-*myc* to the promoters in AASS, BCKDH, ACC, and FAS upon TPO treatment. HBO1 occupancy at these promoters was significantly reduced when c-*myc* was knocked down (Figure 7E, upper panel); knockdown of HBO1 did not affect the binding of c-*myc* to these promoters (Figure 7E, lower panel). Knockdown of either HBO1 or c-*myc* reduced the H3K14 acetylation at these promoters (Figure 7C). An HBO1 enzymatic assay showed that the immunoprecipitated c-*myc* complex contained Geminin-sensitive H3K14Ac acetyltransferase activity (Figure S7B). In the next experiment, endogenous HBO1 knockdown did not affect c-*myc* expression (Figure S7C). HBO1 knockdown repressed c-*myc*-dependent gene activation in lysine catabolism but did not affect the genes involved in fatty acid synthesis (Figure S7D), suggesting that HBO1 plays a more important role in c-*myc*-mediated gene activation than in gene repression.

Both H3K14 Acetylation and H3K27 Trimethylation Are Required for c-*myc*-Mediated Repression of Genes Encoding Enzymes Involved in Fatty Acid Synthesis

Our observation that H3K14 was acetylated at c-*myc* binding sites, regardless of whether the genes were activated or repressed, suggests that additional modifications are required to determine the fate of c-*myc* targets. In the quantitative ChIP (qChIP) experiment with CD110+ cells, TPO increased H3K14Ac as well as H3K27 trimethylation (H3K27me3) on the ACC and FAS promoters. In the promoters of AASS and BCKDH, TPO increased H3K14Ac but not H3K27me3 (Figure 7F). Consistently, confocal imaging showed only partial overlap of c-*myc*

Figure 6. Overcoming Chemoresistance of CD110+TICs by Abolishing the Lys → Glu Protective Mechanism

(A–C) Schematic representation (A) of the parental lentiviral backbone (upper), the subsequent cloning intermediate (middle), and the final dual-promoter lentiviral vector (lower) used in this study. CRC102-LM cells transfected with pCRTA were orthotopically implanted into NOG mice and allowed to form obvious tumors in 4 weeks. Mice were randomized into groups (n = 30 each) that received saline, 5-FU (50 mg/kg), Tet (4 mg/kg), or 5-FU+Tet. All treatments were repeated every 28 days for three cycles. Mice were monitored weekly for bioluminescence (B) and percentage of CD110+ cells (C) in primary lesions (upper panel) and liver metastases (lower panel).

(D) GSH level (upper panel) and activity of TOP/FOP reporter plasmid (lower panel) in CD110+ cells from primary lesions and liver metastases.

(E) CD110+ cells in liver metastases from mice receiving saline were incubated ex vivo with 5-FU (20 μM), 5-FU plus 10 nM BSO, or 5-FU plus pGL-DKK1 (upper panel). CD110+ cells in liver metastases from mice receiving Tet treatment were incubated ex vivo with 5-FU (20 μM), 5-FU plus 2 mM GSH, or 5-FU plus Wnt3A conditional medium (lower panel). Cell viability was analyzed by flow cytometry 3 days after treatment.

Values are mean ± SD. **$p < 0.05$.

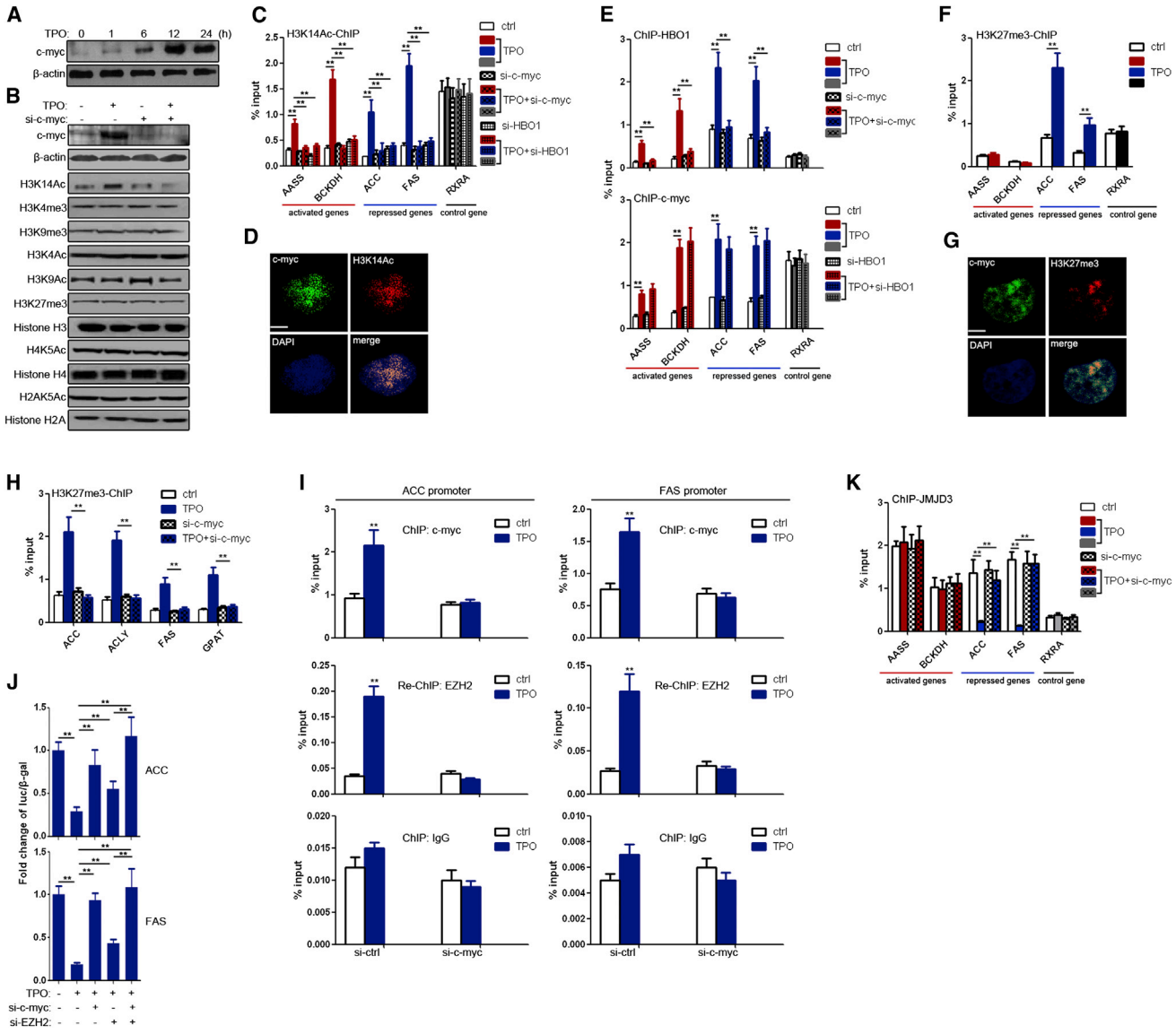

Figure 7. TPO-Induced c-*myc* Coordinates H3K14 Acetylation and H3K27 Trimethylation to Regulate Genes Encoding Enzymes Involved in Lysine Degradation and Fatty Acid Synthesis

(A) After CD110+ cells from CRC102 were treated with 0.1 ng/ml TPO for the indicated times, c-*myc* expression was determined by western blots.

(B) Western blots of different histone markers in CD110+ cells expressing c-*myc* siRNA, following TPO treatment (0.1 ng/ml). Levels of total histone 3, 4, or 2A were used as controls.

(C) CD110+ cells from CRC102 were treated for 6 hr with 0.1 ng/ml TPO and/or siRNA against c-*myc* or HBO1. H3K14 acetylation was analyzed at the indicated promoters by ChIP-qPCR.

(D) A representative confocal image of c-*myc* (green) and acetylated H3K14 (red) in CD110+ cells treated with 0.1 ng/ml TPO for 6 hr.

(E) CD110+ cells from CRC105 were treated as described in Figure 7C; the association of endogenous c-*myc* and HBO1 at the indicated promoters was analyzed with ChIP-qPCR.

(F) CD110+ cells from CRC105 were treated with 0.1 ng/ml TPO for 6 hr, and H3K27 trimethylation was analyzed at the indicated promoters using ChIP-qPCR.

(G) A representative confocal image of c-*myc* (green) and trimethylated H3K27 (red) in CD110+ cells treated with 0.1 ng/ml TPO for 6 hr.

(H) CD110+ cells from CRC102 were treated for 6 hr with 0.1 ng/ml TPO and/or c-*myc* siRNA. H3K27 trimethylation at the indicated promoters was analyzed by ChIP-qPCR.

(I) CD110+ cells from CRC102 were treated for 6 hr with 0.1 ng/ml TPO and/or c-*myc* siRNA; recruitment of EZH2 by c-*myc* on the indicated promoters was determined by sequential ChIP-qPCR. IgG, immunoglobulin G; Re-ChIP, sequential ChIP assay.

(J) CD110+ cells from CRC102 were treated for 6 hr with 0.1 ng/ml TPO and/or siRNA against c-*myc* or EZH2; c-*myc* responsiveness of the indicated promoters was determined by luciferase (luc) reporter assays. β-gal, β-galactosidase.

(K) CD110+ cells from CRC105 were treated for 6 hr with 0.1 ng/ml TPO and/or siRNA against c-*myc*; the association of JMJD3 at the indicated promoters was analyzed with ChIP-qPCR.

Values are mean ± SD. **$p < 0.05$. Scale bars, 5 μm. See also Figure S7.

with H3K27me3 (Figure 7G). Knockdown of c-*myc* abolished TPO-induced changes in H3K27me3 on the promoters of genes related to fatty acid synthesis (Figure 7H). H3K27me3 is associated with gene repression in mammals (Barski et al., 2007). TPO-induced upregulation of H3K27me3 was also observed in the promoters of most other genes encoding enzymes involved in fatty acid synthesis (Figure S7E).

H3K27 methylation is a reversible process that can be catalyzed by either histone methyltransferase EZH2 or demethylases such as the ubiquitously transcribed *TPR* gene on the X chromosome (UTX) and Jumonji-domain-containing protein 3 (JMJD3) (Kuzmichev et al., 2002; Swigut and Wysocka, 2007). UTX was hardly detectable in CD110+ cells and not affected by TPO treatment (Figure S7F). Also, TPO treatment did not affect the expression of EZH2 or JMJD3. We performed sequential qChIP assays using anti-c-*myc* antibody followed by anti-EZH2 antibody on the ACC and FAS promoters. After TPO treatment, EZH2 was pulled down in the anti-c-*myc* ChIP from CD110+ cells but not from the c-*myc* knockdown clones (Figure 7I). A small interfering RNA (siRNA) against c-*myc* increased ACC or FAS promoter luciferase activity (Figure 7J); and concurrent inhibition of EZH2 with a siRNA led to further increase in promoter luciferase activity. TPO treatment also significantly reduced the binding of JMJD3 to the promoters of most genes encoding enzymes in fatty acid synthesis but not the genes encoding enzymes in lysine catabolism (Figures 7K and S7G); such effect was abolished by c-*myc* knockdown. These results indicated that c-*myc* recruits EZH2, as well as displaces JMJD3, to mediate the repression of genes related to fatty acid synthesis.

DISCUSSION

In the current study, transcriptome analysis suggested activation of lysine catabolism in CD110+TICs that drives liver metastasis. This lysine degradation occurs primarily via the saccharopine pathway in the liver (Higashino et al., 1965). Under normal conditions, lysine degradation provides acetyl-CoA to the citric acid cycle and fatty acid synthesis (Papes et al., 1999). We found that, in CD110+TICs, acetyl-CoA is channeled to acetylate LRP6 on K802 in a p300-dependent manner. This acetylation recruits and activates CKs to phosphorylate LRP6, which, in turn, activates β-catenin-dependent Wnt signaling and regulates self-renewal in CD110+TICs (Vermeulen et al., 2010). In this sense, lysine catabolism initiates liver colonization by coordinating the production of acetyl-CoA. Our findings must be interpreted within proper context: the lysine catabolism is likely to be important only at the early stages of liver metastasis of CRC and not essential for bulk growth of liver metastases. We detected AASS expression in tissue from resected liver lesions (macrometastases) from CRC patients, and we found suppressed AASS expression in tumor-adjacent liver tissues. We speculate, albeit with limited evidence, that the suppression of AASS expression in tumor-adjacent liver tissue reduces lysine utilization in the body and is not released after the establishment of metastatic nodules, thus providing enough lysine to help metastatic CD110+TICs from primary lesions or metastatic sites to form new metastases in the liver. Further studies are required to define whether this is attributed to persistence of mutual crosstalk between primary tumor and liver microenvironment.

Liver ischemia produced by metastatic tumor cells as they arrest in hepatic microcirculation generates ROS and reactive nitrogen species, which, in turn, could act as a barrier to liver colonization (Jessup et al., 1999). Highly glycolytic TICs typically produce reducing species in order to strengthen antioxidant defenses (Mao et al., 2013). Paradoxically, we found that CD110+TICs exhibit spontaneous apoptosis when cultured with $TPO^{-/-}$ ischemic livers. It is possible that, in liver metastasis of CRC, lysine catabolism provides an antioxidant strategy because the saccharopine pathway may serve to generate glutamate (Papes et al., 2001), which promotes GSH synthesis by enhancing cystine uptake (Lewerenz et al., 2013) and by competing with GSH in the regulatory site of γGCS (Richman and Meister, 1975). In this way, lysine catabolism could increase the ability of CD110+TICs to maintain redox balance during liver colonization. Increased GSH synthesis may confer an additional benefit to the cancer: GSH could conjugate to, and thus activate, anticancer drugs through the action of GSH S-transferases (Liu et al., 2010). Our data well explain why most CRC patients undergo hepatic relapse even after receiving curative resection and radiochemotherapy. Disrupting the lysine-glutamate flow represents a novel therapeutic approach to prevent post-therapeutic recurrence.

TPO could rapidly induce c-*myc* expression in CD110+TICs (Chanprasert et al., 2006), and this induction correlates with large-scale changes in histone modifications (Knoepfler et al., 2006). Our results suggest that direct interaction between c-*myc* and HBO1, a lysine acetyltransferase essential for H3K14 acetylation and multipotency in embryonic stem cells (Kueh et al., 2011), induces local H3K14 acetylation, regardless of whether the target genes are activated or repressed. We showed that HBO1 is broadly required for c-*myc*-mediated gene *activation* but not c-*myc*-dependent gene *repression*. We also found increased H3K27 trimethylation in repressed targets of c-*myc*. For many target genes, c-*myc* represses expression by recruiting H3K27 methyltransferase EZH2, as well as by displacing the demethylase JMJD3. Based on these results, we speculate that repressive H3K27 trimethylation overrides stimulatory H3K14 acetylation, resulting in gene silencing in c-*myc*-associated chromatin. Such a regulatory system is, in some way, similar to bivalent domains in embryonic-stem-cell developmental genes (Bernstein et al., 2006), where trimethylation of H3K27 and of H3K4 occur together. In this system, the target genes are silenced but poised for activation, ensuring rapid transition between metabolic states needed to support the dynamic interplay between TIC pluripotency and differentiation during liver colonization.

EXPERIMENTAL PROCEDURES

Cell Culture

Human CRC tissues were obtained with informed consent and in accordance with the ethical standards of the Changzheng Hospital Institutional Review Board. Primary CRC cells (CRC102, CRC105, and CRC108) and their liver-specific variants (CRC102-LM, CRC105-LM, and CRC108-LM) were maintained as previously described (Gao et al., 2013). CRC105 cells have wild-type adenomatous polyposis coli (APC) and β-catenin, while CRC102 and CRC108 cells harbor mutated APC (codon 1197, CTC → TTT) and β-catenin (codon 41, ACC → GCC), respectively. When magnetic-activated cell sorting (MACS) was used to sort for CD110+ cells, dissociated tumor cells were incubated

with a monoclonal CD110 antibody labeled with MicroBeads (Miltenyi Biotec) for 30 min at 4°C, followed by cleavage of the MicroBeads. For Lys deprivation, cells were cultured with lysine-depleted DMEM (Thermo Scientific). Lysine, α-aminoadipate, α-ketoadipate, and acetoacetate were purchased from Sigma-Aldrich. For siRNA inhibition studies, cells were transfected with validated human AASS, HMGCL, LRP6, p300, c-*myc*, HBO1, and EZH2 siRNA or negative control siRNA (Ambion) at a final concentration of 100 nM in the presence of an Oligofectamine reagent (Invitrogen).

Animal Studies

All animal protocols were approved by the Institutional Animal Care and Use Committee for Second Military Medical University. The thrombopoietin null ($TPO^{-/-}$) mice were purchased from Genentech. All in vivo experiments were performed in 4-week-old NOG mice. To generate orthotopic tumors, we injected suspensions of the indicated cells into the cecal wall after laparotomy. In experimental metastasis assays, 1×10^5 CD110+ cells were injected into the lateral tail vein of NOG mice. The GFP-lentiviral transduction facilitated bioluminescence monitoring (Nikon, Nippon Kogaku) of tumor size and incidence of liver metastases.

Statistical Analysis

All statistical analyses were carried out with SPSS software. Disease-free survival and overall survival curves were estimated with the Kaplan-Meier method. ANOVA, Student's t test, and Dunnett's multiple comparison tests were used to compare mean values. Data are presented as mean ± SD. A p value < 0.05 was defined as statistically significant.

ACCESSION NUMBERS

The GEO accession number for human datasets is GEO: GSE64595.

SUPPLEMENTAL INFORMATION

Supplemental Information includes Supplemental Experimental Procedures and seven figures and can be found with this article online at http://dx.doi.org/10.1016/j.stem.2015.05.016.

AUTHOR CONTRIBUTIONS

Conceptualization, D.W. and Q.L.; Methodology, Z.W., W.G., and Q.L.; Investigation, Z.W., Y.X., Z.M., Z.H., W.G., and X.Z.; Writing—Original Draft, Z.W. and Q.L.; Writing—Review And Editing, Z.W., W.G., and Q.L.; Funding Acquisition, W.G. and Q.L.; Resources, Z.M., Z.H., and C.G.; Supervision: Q.L.

ACKNOWLEDGMENTS

This work was supported by grants from the National Nature Science Foundation of China (81372350 and 81172099).

Received: January 25, 2015
Revised: April 26, 2015
Accepted: May 29, 2015
Published: July 2, 2015

REFERENCES

Barski, A., Cuddapah, S., Cui, K., Roh, T.Y., Schones, D.E., Wang, Z., Wei, G., Chepelev, I., and Zhao, K. (2007). High-resolution profiling of histone methylations in the human genome. Cell *129*, 823–837.

Bernstein, B.E., Mikkelsen, T.S., Xie, X., Kamal, M., Huebert, D.J., Cuff, J., Fry, B., Meissner, A., Wernig, M., Plath, K., et al. (2006). A bivalent chromatin structure marks key developmental genes in embryonic stem cells. Cell *125*, 315–326.

Bilic, J., Huang, Y.L., Davidson, G., Zimmermann, T., Cruciat, C.M., Bienz, M., and Niehrs, C. (2007). Wnt induces LRP6 signalosomes and promotes dishevelled-dependent LRP6 phosphorylation. Science *316*, 1619–1622.

Chanprasert, S., Geddis, A.E., Barroga, C., Fox, N.E., and Kaushansky, K. (2006). Thrombopoietin (TPO) induces c-myc expression through a PI3K- and MAPK-dependent pathway that is not mediated by Akt, PKCzeta or mTOR in TPO-dependent cell lines and primary megakaryocytes. Cell. Signal. *18*, 1212–1218.

Davidson, G., Wu, W., Shen, J., Bilic, J., Fenger, U., Stannek, P., Glinka, A., and Niehrs, C. (2005). Casein kinase 1 gamma couples Wnt receptor activation to cytoplasmic signal transduction. Nature *438*, 867–872.

Fox, N., Priestley, G., Papayannopoulou, T., and Kaushansky, K. (2002). Thrombopoietin expands hematopoietic stem cells after transplantation. J. Clin. Invest. *110*, 389–394.

Gao, W., Chen, L., Ma, Z., Du, Z., Zhao, Z., Hu, Z., and Li, Q. (2013). Isolation and phenotypic characterization of colorectal cancer stem cells with organ-specific metastatic potential. Gastroenterology *145*, 636–646.e5.

Higashino, K., Tsukada, K., and Lieberman, I. (1965). Saccharopine, a product of lysine breakdown by mammalian liver. Biochem. Biophys. Res. Commun. *20*, 285–290.

Hong, Y., Dumènil, D., van der Loo, B., Goncalves, F., Vainchenker, W., and Erusalimsky, J.D. (1998). Protein kinase C mediates the mitogenic action of thrombopoietin in c-Mpl-expressing UT-7 cells. Blood *91*, 813–822.

Jessup, J.M., Battle, P., Waller, H., Edmiston, K.H., Stolz, D.B., Watkins, S.C., Locker, J., and Skena, K. (1999). Reactive nitrogen and oxygen radicals formed during hepatic ischemia-reperfusion kill weakly metastatic colorectal cancer cells. Cancer Res. *59*, 1825–1829.

Kaochar, S., and Tu, B.P. (2012). Gatekeepers of chromatin: Small metabolites elicit big changes in gene expression. Trends Biochem. Sci. *37*, 477–483.

Kaser, A., Brandacher, G., Steurer, W., Kaser, S., Offner, F.A., Zoller, H., Theurl, I., Widder, W., Molnar, C., Ludwiczek, O., et al. (2001). Interleukin-6 stimulates thrombopoiesis through thrombopoietin: role in inflammatory thrombocytosis. Blood *98*, 2720–2725.

Knoepfler, P.S., Zhang, X.Y., Cheng, P.F., Gafken, P.R., McMahon, S.B., and Eisenman, R.N. (2006). Myc influences global chromatin structure. EMBO J. *25*, 2723–2734.

Knüpfer, H., and Preiss, R. (2010). Serum interleukin-6 levels in colorectal cancer patients—a summary of published results. Int. J. Colorectal Dis. *25*, 135–140.

Koch, C.M., Andrews, R.M., Flicek, P., Dillon, S.C., Karaöz, U., Clelland, G.K., Wilcox, S., Beare, D.M., Fowler, J.C., Couttet, P., et al. (2007). The landscape of histone modifications across 1% of the human genome in five human cell lines. Genome Res. *17*, 691–707.

Kueh, A.J., Dixon, M.P., Voss, A.K., and Thomas, T. (2011). HBO1 is required for H3K14 acetylation and normal transcriptional activity during embryonic development. Mol. Cell. Biol. *31*, 845–860.

Kuzmichev, A., Nishioka, K., Erdjument-Bromage, H., Tempst, P., and Reinberg, D. (2002). Histone methyltransferase activity associated with a human multiprotein complex containing the Enhancer of Zeste protein. Genes Dev. *16*, 2893–2905.

Lewerenz, J., Hewett, S.J., Huang, Y., Lambros, M., Gout, P.W., Kalivas, P.W., Massie, A., Smolders, I., Methner, A., Pergande, M., et al. (2013). The cystine/glutamate antiporter system x(c)(-) in health and disease: from molecular mechanisms to novel therapeutic opportunities. Antioxid. Redox Signal *18*, 522–555.

Liu, Y.H., Di, Y.M., Zhou, Z.W., Mo, S.L., and Zhou, S.F. (2010). Multidrug resistance-associated proteins and implications in drug development. Clin. Exp. Pharmacol. Physiol. *37*, 115–120.

Mao, P., Joshi, K., Li, J., Kim, S.H., Li, P., Santana-Santos, L., Luthra, S., Chandran, U.R., Benos, P.V., Smith, L., et al. (2013). Mesenchymal glioma stem cells are maintained by activated glycolytic metabolism involving aldehyde dehydrogenase 1A3. Proc. Natl. Acad. Sci. USA *110*, 8644–8649.

Martin, T.G., 3rd, Somberg, K.A., Meng, Y.G., Cohen, R.L., Heid, C.A., de Sauvage, F.J., and Shuman, M.A. (1997). Thrombopoietin levels in patients with cirrhosis before and after orthotopic liver transplantation. Ann. Intern. Med. *127*, 285–288.

Niehrs, C. (2006). Function and biological roles of the Dickkopf family of Wnt modulators. Oncogene *25*, 7469–7481.

Ogryzko, V.V., Schiltz, R.L., Russanova, V., Howard, B.H., and Nakatani, Y. (1996). The transcriptional coactivators p300 and CBP are histone acetyltransferases. Cell *87*, 953–959.

Oskarsson, T., Batlle, E., and Massagué, J. (2014). Metastatic stem cells: sources, niches, and vital pathways. Cell Stem Cell *14*, 306–321.

Pang, R., Law, W.L., Chu, A.C., Poon, J.T., Lam, C.S., Chow, A.K., Ng, L., Cheung, L.W., Lan, X.R., Lan, H.Y., et al. (2010). A subpopulation of CD26+ cancer stem cells with metastatic capacity in human colorectal cancer. Cell Stem Cell *6*, 603–615.

Papes, F., Kemper, E.L., Cord-Neto, G., Langone, F., and Arruda, P. (1999). Lysine degradation through the saccharopine pathway in mammals: involvement of both bifunctional and monofunctional lysine-degrading enzymes in mouse. Biochem. J. *344*, 555–563.

Papes, F., Surpili, M.J., Langone, F., Trigo, J.R., and Arruda, P. (2001). The essential amino acid lysine acts as precursor of glutamate in the mammalian central nervous system. FEBS Lett. *488*, 34–38.

Richman, P.G., and Meister, A. (1975). Regulation of gamma-glutamyl-cysteine synthetase by nonallosteric feedback inhibition by glutathione. J. Biol. Chem. *250*, 1422–1426.

Sangeetha, P., Das, U.N., Koratkar, R., and Suryaprabha, P. (1990). Increase in free radical generation and lipid peroxidation following chemotherapy in patients with cancer. Free Radic. Biol. Med. *8*, 15–19.

Swigut, T., and Wysocka, J. (2007). H3K27 demethylases, at long last. Cell *131*, 29–32.

Tang, D.G. (2012). Understanding cancer stem cell heterogeneity and plasticity. Cell Res. *22*, 457–472.

Tao, G.Z., Lehwald, N., Jang, K.Y., Baek, J., Xu, B., Omary, M.B., and Sylvester, K.G. (2013). Wnt/β-catenin signaling protects mouse liver against oxidative stress-induced apoptosis through the inhibition of forkhead transcription factor FoxO3. J. Biol. Chem. *288*, 17214–17224.

Vermeulen, L., De Sousa E Melo, F., van der Heijden, M., Cameron, K., de Jong, J.H., Borovski, T., Tuynman, J.B., Todaro, M., Merz, C., Rodermond, H., et al. (2010). Wnt activity defines colon cancer stem cells and is regulated by the microenvironment. Nat. Cell Biol. *12*, 468–476.

Vigon, I., Mornon, J.P., Cocault, L., Mitjavila, M.T., Tambourin, P., Gisselbrecht, S., and Souyri, M. (1992). Molecular cloning and characterization of MPL, the human homolog of the v-mpl oncogene: identification of a member of the hematopoietic growth factor receptor superfamily. Proc. Natl. Acad. Sci. USA *89*, 5640–5644.

Visvader, J.E., and Lindeman, G.J. (2008). Cancer stem cells in solid tumours: accumulating evidence and unresolved questions. Nat. Rev. Cancer *8*, 755–768.

Voutsadakis, I.A. (2014). Thrombocytosis as a prognostic marker in gastrointestinal cancers. World J. Gastrointest. Oncol. *6*, 34–40.

Wang, F.S., Shao, Z.G., Zhang, J.L., and Liu, Y.F. (2012). Colorectal liver metastases rarely occur in patients with chronic hepatitis virus infection. Hepatogastroenterology *59*, 1390–1392.

Yuan, L.W., and Gambee, J.E. (2000). Phosphorylation of p300 at serine 89 by protein kinase C. J. Biol. Chem. *275*, 40946–40951.